Presented at 70th International Astronautical Congress (IAC), Washington D.C., United States, 21-25 October 2019
https://iafastro.directory/iac/paper/id/49094/summary/

IAC-19-C1.7.6

Autonomous Navigation and Guidance for CubeSats to Flyby Near-Earth Asteroids

Pablo Machuca[a,*], Joan Pau Sánchez[b]

[a] *Space Research Group, Cranfield University, College Road, Cranfield, Bedfordshire, United Kingdom MK43 0AL*, p.machuca@cranfield.ac.uk
[b] *Space Research Group, Cranfield University, College Road, Cranfield, Bedfordshire, United Kingdom MK43 0AL*, jp.sanchez@cranfield.ac.uk
* Corresponding Author

Abstract

Recent advancements in CubeSat technology unfold new mission ideas and the possibility to lower the cost of space exploration. Exploiting the natural dynamics around the Sun-Earth barycentric Lagrange points, minimal-ΔV trajectories to flyby asteroids appear which are compatible with current CubeSat propulsive capabilities. Ground operations costs for an interplanetary CubeSat, however, still represent a major challenge towards low-cost missions; hence certain levels of autonomy are desirable. Considering the limited allocation of sensors and actuators in CubeSats, and their limited performance, Monte Carlo simulations are implemented to understand the flyby accuracies that can be achieved through autonomous navigation and guidance. Primary sources of error analyzed in this study include: (1) uncertainties in the departure conditions, (2) errors in the propulsive maneuvers, (3) errors in the observations, and (4) uncertainties in the ephemeris of the target asteroid. An autonomous navigation and guidance strategy is proposed and evaluated, employing observations of the Sun, visible planets and of the target asteroid, and two trajectory correction maneuvers along the trajectory. Flyby accuracies below 100 km are found possible if the mission characteristics are suitable in terms of available ΔV, on-board asteroid visibility time, mission duration, and asteroid ephemeris uncertainty before the mission. Ultimately, this study assesses the readiness level of current CubeSat technology to autonomously flyby near-Earth asteroids, with realistic component specifications and modeling of relevant errors and uncertainties. The effect of the different mission factors on the final flyby accuracies is evaluated, and a feasible autonomous navigation and guidance strategy is proposed in the effort to reduce ground operations and overall mission costs.

Keywords: Autonomous navigation and guidance; interplanetary CubeSats; near-Earth asteroids

Nomenclature

ΔV	Velocity increment
H	Absolute magnitude
$\underline{\boldsymbol{I}}_{ixi}$	Identity matrix of size i
$\underline{\boldsymbol{P}}_a$	Covariance matrix of variable a
$\underline{\boldsymbol{\phi}}(t_2, t_1)$	State-transition matrix from time t_1 to time t_2
$\underline{\boldsymbol{Q}}_a$	Covariance matrix associated to event a
$\underline{\boldsymbol{Q}}_{a,b}$	Elements in matrix $\underline{\boldsymbol{Q}}_a$ associated to variable b
$\boldsymbol{r}$	Position vector
σ_a	Standard deviation of variable a
t	Time variable
ε, θ	Elevation and azimuth representing direction vectors
r_s,	Sum of distances from observer to pair of planets
θ_s,	Angle between lines of sight from observer to pair of planets
$\boldsymbol{r}$	Velocity vector
V	Visual magnitude
$\boldsymbol{x}$	State vector (Cartesian position and velocity)
$\hat{\boldsymbol{x}}, \hat{\boldsymbol{y}}, \hat{\boldsymbol{z}}$	Cartesian unit vectors defining an inertial reference frame
$\underline{\boldsymbol{0}}_{ixi}$	Zero matrix of size i
bold	Represents vectors
bold	Represents matrices

Acronyms/Abbreviations

ADCS	Attitude determination and control system
BCT	Blue Canyon Technologies
EMB	Earth-Moon barycenter
L1, L2	First and second Sun-EMB Lagrange points
PUC	Propulsion Unit for CubeSats
STM	State-transition matrix
TCM	Trajectory correction maneuver
U	CubeSat basic unit (10 cm x 10 cm x 10 cm)

1. Introduction

Low-ΔV trajectories, suitable for CubeSat propulsive capabilities, to flyby near-Earth asteroids can be designed

from the Sun-Earth barycentric Lagrange points [1]. Certain levels of autonomy, however, are desirable for interplanetary CubeSat missions in the interest of low mission budgets. A feasibility analysis of an asteroid flyby mission using autonomous CubeSats is hence performed here.

An autonomous navigation and guidance strategy is proposed and assessed in search of a reduced use of ground stations. In view of the limited number of sensors on board CubeSats, the navigation strategy employs only observations of the Sun, visible planets and of the target asteroid, which could be collected by an on-board sun sensor and a star tracker. The guidance strategy considers two trajectory correction maneuvers executed before and after the asteroid becomes visible to the CubeSat. A heuristic to determine the time of execution of these correction maneuvers is introduced here. Navigation and guidance algorithms furthermore propagate trajectories and compute correction maneuvers employing prestored state-transition matrices only, which is more suitable for the limited on-board computational power than numerical integration. No complex optimization algorithms are involved either in the computation of correction maneuvers.

Monte Carlo simulations are performed to understand the flyby accuracies that can be achieved by an autonomous CubeSat, and results are compared to those of the simple one-maneuver guidance strategy employed in [2] for the same mission concept. Analysis includes realistic system specifications and modeling of errors and uncertainties in: (1) departure conditions, (2) propulsive maneuvers, (3) observations, and (4) asteroid ephemeris.

The mission scenario is introduced in Section 2, modeling of errors and uncertainties is described in Section 3, the autonomous navigation and guidance strategies are presented in Section 4, and analysis and discussion of the results can be found in Section 5.

2. Mission scenario

The mission concept considered in this analysis assumes a CubeSat is initially parked in a halo orbit around the first or the second Sun-EMB Lagrange points. From these L1/L2 halo orbits, the CubeSat executes its own propulsive maneuvers to flyby a near-Earth asteroid while performing autonomous navigation and guidance. For reference, the design of CubeSat-compatible asteroid flyby trajectories from the Sun-EMB Lagrange points is studied in [1], along with a more detailed discussion on the mission scenario. Impulsive flyby trajectories computed in [1] (in an ephemeris dynamical model) are used in this study as baseline trajectories, which are also designed to last less than 150 days after departure from L1/L2 and to employ less than 80 m/s of ΔV.

Analysis in this study focuses on the feasibility of performing autonomous navigation and guidance along these asteroid flyby trajectories. The goal of the guidance campaign is to eliminate deviations from the baseline trajectory in order to reach the same relative encounter position at the same time—unlike the encounter velocity, which is not corrected to any particular target.

Following the mission scenario in [1], the spacecraft considered in the analysis is a 3U CubeSat platform with a total ΔV budget of 80 m/s, according to current CubeSat capabilities [3]. This same ΔV is allocated in this study for both: maneuvers along the baseline trajectory and trajectory correction maneuvers. Observations employed for navigation include: (1) observations of the Sun, (2) observations of visible planets, and (3) observations of the target asteroid. These observations are assumed to be collected through a coarse sun sensor (observations of the Sun), and a star tracker (observations of planets and asteroid). According to the systems analysis performed in [2], this is identified as a suitable set of instruments for the mission scenario considering the allocation of other subsystems and of the science payload.

Larger CubeSat platforms could potentially allocate more numerous or higher-performance components, but a 3U CubeSat is considered here in search of the minimal spacecraft platform that would enable an asteroid flyby mission, and in contrast to previous asteroid mission studies using 6U or larger spacecraft [4,5].

Subsystems and component specifications relevant to the analysis here performed include those of the propulsion system, attitude determination and control system, coarse sun sensor, and star tracker. Based on the mission study in [2], Table 1 summarizes the component selection and performance assumed in the navigation and guidance analysis.

Similarly to the analysis in [1] and [2], a constraint is also added on the minimum size of the target asteroids: larger 100 meters in diameter (absolute magnitude $H \leq 22.5$). This constraint is particularly relevant for asteroid detection as it will determine how long before the flyby the asteroid can be observed, and longer asteroid observation times ultimately drive navigation and flyby accuracies.

Additionally, it is assumed that, if the target asteroid can be observed from Earth before departure from L1/L2, new ground observations of the asteroid are collected and employed to improve the accuracy of asteroid ephemeris. These updated asteroid ephemerides are then made available to the CubeSat prior to its L1/L2 departure.

3. Modeling of errors and uncertainties

Monte Carlo simulations are performed to understand the flyby accuracies that can be achieved autonomously by a CubeSat. Errors and uncertainties introduced in the analysis include: (1) uncertainties in the CubeSat's initial position and velocity, (2) errors in the propulsive maneuvers, (3) errors in the observations of the Sun, planets and target asteroid, and (4) uncertainties in the trajectory of the asteroid.

Table 1. Component selection and assumed performance

Component	Assumed performance		Comments
	Characteristic	Value	
VACCO's 5-mN 0.5U Propulsion Unit for CubeSats	ΔV magnitude accuracy	±1% (3σ)	Reported uncertainty in magnitude is <5% (3σ) but includes experimental measurement errors [6]. Optimistic value of ±1% (3σ) is employed and derived as a systems requirement.
	ΔV directional accuracy	±0.1 deg (3σ)	No flutter (directional) noise is reported for VACCO's PUC, but a ±0.1 deg (3σ) accuracy is employed and derived as a systems requirement, based on reported accuracies of LISA Pathfinder's cold gas and ion micro-thrusters [7,8]: ±0.15 deg (3σ), and accuracies of mN-level ion thrusters: ±0.1 deg (3σ) [9].
BCT's 0.5U XACT unit	Pointing knowledge	±0.01 deg (3σ)	Reported boresight pointing knowledge of star tracker integrated in BCT's XACT is ±0.02 deg (3σ), and cross-axis knowledge is ±0.006 deg (3σ) [10]. Value of ±0.01 deg (3σ) is employed as cross-axis performance is most relevant to the analysis.
	Pointing accuracy	±0.1 deg (3σ)	Reported boresight accuracy in LEO is ±0.02 deg (3σ), and cross-axis accuracy is ±0.006 deg (3σ) [11]. Conservative value of ±0.1 deg (3σ) is employed, which could account for the unavailability of magnetorquers and magnetometers in deep space.
	Limiting magnitude	11	Reported limiting magnitude of star tracker integrated in BCT's XACT is 7.0 with a 5-Hz update rate [10]. Optimistic value of 11 is assumed possible through longer exposure times and is derived as a systems requirement.
	Centroiding accuracy	±0.01 deg (3σ)	Centroiding accuracy is expected to be significantly better than cross-axis pointing knowledge of ±0.006 deg (3σ) [10]. Conservative value of ±0.01 deg (3σ) is assumed for observations of planets and of the asteroid considering long exposure times for asteroid detection.
Hyperion Technologies' sun sensor	Accuracy	±1 deg (3σ)	Reported accuracy is <1 deg (3σ) [12].

3.1. Uncertainty in initial state

The uncertainty in the initial state is assumed to be 30 km (3σ) in position, and 30 cm/s (3σ) in velocity. These values are drawn from the autonomous navigation study for the 12U mission LUMIO around the second Earth-Moon Lagrange point [13]. Whether achieved autonomously or through ground-based tracking, this initial state uncertainty is derived as an initial requirement for the mission.

The uncertainty in the initial position and velocity of each Monte Carlo case is defined in spherical coordinates by, respectively, one radial and two angular uncertainties. The radial uncertainty is characterized by the corresponding normally-distributed uncertainty in position or velocity, and the two angular uncertainties are defined as uniform random errors spanning over a whole sphere (Fig. 1). As a consequence, the (uncorrelated) initial covariance matrices in position and velocity are

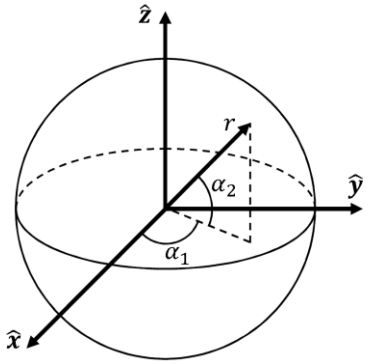

Fig. 1. Representation of uncertainty in initial state in spherical coordinates

defined in Cartesian coordinates as $\underline{\boldsymbol{P}}_{\bar{r}\bar{r}}(t_0) = \left(\frac{10\ km}{\sqrt{3}}\right)^2 \cdot \underline{\boldsymbol{I}}_{3x3}$ and $\underline{\boldsymbol{P}}_{\bar{v}\bar{v}}(t_0) = \left(\frac{10\ cm/s}{\sqrt{3}}\right)^2 \cdot \underline{\boldsymbol{I}}_{3x3}$.

3.2. Error in propulsive maneuvers

Errors in the propulsive maneuvers are modeled based on the component performance specified in Table 1. Propulsive maneuvers are modeled as impulsive and have errors both in magnitude and in direction. The magnitude error is driven by the normally-distributed magnitude accuracy of the thruster, and the direction error is cumulative and due to (1) pointing accuracy of the ADCS, and (2) directional accuracy of the thruster (Fig. 2). Both angular errors are normally distributed.

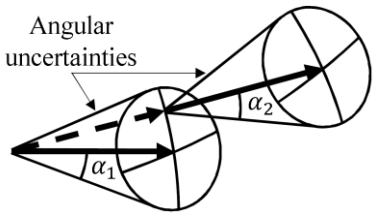

Fig. 2. Representation of directional error due to two cumulative angular errors

Uncertainties in the propulsive maneuvers also introduce uncertainties in the estimation of the CubeSat's trajectory. These uncertainties are accounted for as process noise when performing on-board navigation, as described in Section 4.1. This process noise, $\underline{\boldsymbol{Q}}_{man}$, is assumed to influence only the velocity components of the CubeSat's covariance matrix (see Eq. (1)).

$$\underline{\boldsymbol{Q}}_{man} = \begin{bmatrix} \underline{\mathbf{0}}_{3x3} & \underline{\mathbf{0}}_{3x3} \\ \underline{\mathbf{0}}_{3x3} & \underline{\boldsymbol{Q}}_{man,\boldsymbol{vv}} \end{bmatrix} \quad (1)$$

Computation of matrix $\underline{\boldsymbol{Q}}_{man,\boldsymbol{vv}}$ involves representing the matrix in some auxiliary reference frame and then rotating that matrix to express it in the inertial reference frame. The auxiliary reference frame has its x-axis aligned with the direction vector of the nominal maneuver, and the y- and z-axes are contained in the normal plane.

In this auxiliary reference frame, matrix $\underline{\boldsymbol{Q}}_{man,\boldsymbol{vv}}$ can be expressed as in Eq. (2) (including only first-order terms, and assuming uncorrelated angular errors) [14].

$$\underline{\boldsymbol{Q}}_{man,\boldsymbol{vv}} = |\Delta \boldsymbol{v}_{man}|^2 \cdot \begin{bmatrix} \sigma_{mag}^2 & 0 & 0 \\ 0 & \sigma_\alpha^2 & 0 \\ 0 & 0 & \sigma_\alpha^2 \end{bmatrix} \quad (2)$$

where $|\Delta \boldsymbol{v}_{man}|$ is the magnitude of the nominal propulsive maneuver, σ_{mag} is the per-one standard deviation in the magnitude of the maneuver, and $\sigma_\alpha^2 = \left(\sigma_{\alpha_1}/\sqrt{2}\right)^2 + \left(\sigma_{\alpha_2}/\sqrt{2}\right)^2$ is the cumulative angular covariance due to pointing error of the ADCS and directional error of the thruster (projected on the y- and z-axes).

3.3. Error in observations

Observations in this study are assumed to be collected by two different instruments: sun sensor and star tracker. Both instruments provide directional information (two angles) of the observed bodies. On the one hand, errors in the direction of the Sun are cumulative and due to (1) pointing knowledge of the ADCS, and (2) accuracy of the sun sensor. On the other hand, errors in the direction of the planets and of the target asteroid are also cumulative and due to (1) pointing knowledge of the ADCS, and (2) centroiding accuracy of the star tracker. All directional errors are normally distributed and accumulated as represented in Fig. 2.

Uncertainties in the observations directly impact the quality of the on-board navigation, which is accounted for by the observation-error covariance matrix, $\underline{\boldsymbol{Q}}_{obs}$. In order to calculate this matrix, it is necessary to specify first how direction vectors from the CubeSat to the observed bodies are represented. Direction vectors are described in this study by two angles: azimuth and elevation. The azimuth angle, θ, is contained in the inertial x-y plane and defined with respect to the x-axis, and the elevation angle, ε, is defined with respect to the x-y plane (similar to angles α_1 and α_2 in Fig. 1).

This selection of angles results in an observation-error covariance matrix such as that described in Eq. (3) [14].

$$\underline{\boldsymbol{Q}}_{obs} = \begin{bmatrix} \sigma_\theta^2 & \sigma_{\theta\varepsilon} \\ \sigma_{\theta\varepsilon} & \sigma_\varepsilon^2 \end{bmatrix} = \begin{bmatrix} (\sigma_\alpha/\cos(\varepsilon))^2 & 0 \\ 0 & \sigma_\alpha^2 \end{bmatrix} \quad (3)$$

where σ_α^2 is defined as in Section 3.2 but substituting the observations' angular errors instead. Through this matrix, it is clear that poor azimuth information can be retrieved at large elevation angles as a consequence of a singularity in the selected Euler angle representation. However, given that the motions of the CubeSat, planets and asteroids are close to the ecliptic plane, elevation angles of the observations shall remain small.

3.4. Uncertainty in asteroid ephemeris

Asteroid ephemerides are retrieved in this study through JPL's Horizons telnet interface [15] and propagated in time in an ephemeris dynamical model. Uncertainties in these trajectories are obtained through ESA's NEODyS-2 website [16] in the form of covariance matrices. These covariance matrices are provided at predetermined dates and, in this study, they are linearly propagated in time through the STM associated to the asteroids' nominal, reference trajectories (Eq. (4)).

$$\underline{\boldsymbol{P}}(t_2) = \underline{\boldsymbol{\phi}}(t_2, t_1) \cdot \underline{\boldsymbol{P}}(t_1) \cdot \underline{\boldsymbol{\phi}}(t_2, t_1)^T \quad (4)$$

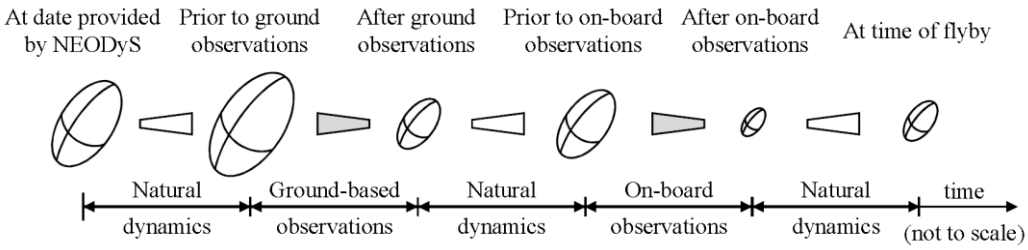

Fig. 3. Uncertainty in asteroid ephemeris along time (including ground-based and on-board observations)

Table 2. Allocated time for ground-based and on-board navigation phases

Type of observation		From	Until	Every
Ground-based observations of asteroid		Asteroid's visual magnitude from Earth V≤22	Past 10 days	24 hours
On-board navigation, Phase 1	Observations of Sun Observations of planets	Departure from L1/L2 plus 24 hours	Asteroid's visual magnitude from CubeSat V≤11 minus 24 hours	6 hours
On-board navigation, Phase 2	Observations of Sun Observations of asteroid	Asteroid's visual magnitude from CubeSat V≤11 plus 30 minutes	End of on-board navigation*	30 minutes

* On-board navigation ends 15 minutes before last trajectory correction maneuver is performed (see Section 4.2).

As mentioned in Section 2, if the target asteroid can be observed from Earth prior to the CubeSat's L1/L2 departure, then new ground observations are assumed to be collected to reduce uncertainties in asteroid ephemeris. Observability from Earth is determined possible if the visual magnitude of the asteroid is below or equals 22: V≤22, and a solar exclusion angle of 50 degrees is also imposed.

Based on the statistical analysis of asteroid observations in [17], an accuracy of 0.388 arcsec (3σ) is assumed for the new CCD observations of the asteroid, with an observation-error covariance matrix such as that in Eq. (3). One optical astrometric observation per day over up to ten days is assumed to be collected during the last observation window prior to the departure. These new observations are processed by a least squares estimator [18] using as *a priori* estimation the covariance matrix provided by NEODyS (propagated in time until the corresponding observation window).

This updated asteroid ephemeris is then employed by the CubeSat as *a priori* estimation during on-board navigation. On-board observations of the asteroid are collected by the CubeSat's star tracker every 30 minutes, starting 30 minutes after the asteroid's visual magnitude becomes smaller than or equals the star tracker's limiting magnitude: V≤11 (refer to Table 1). The error in these observations is modeled as described in Section 3.3. These new on-board observations are also processed by a least squares estimator and help reduce the uncertainty in relative CubeSat-asteroid flyby position.

A schematic of the behavior of the uncertainty in asteroid ephemeris along time is provided in Fig. 3, considering new ground observations and on-board navigation. The timeline of ground-based and on-board observations is also summarized in Table 2.

4. Autonomous navigation and guidance

Navigation and guidance are assumed to be performed autonomously throughout the asteroid flyby trajectory: from L1/L2 departure to the flyby. Considering a limited computational capability on board the CubeSat, and in order to reduce the computational demand, it is further assumed that all on-board navigation and guidance algorithms propagate the estimated trajectories of the CubeSat and of the asteroid (and associated covariance matrices) using an STM-based propagation rather numerically integrating their equations of motion. No complex optimization algorithms are employed in the computation of correction maneuvers either.

The state-transition matrices employed for trajectory propagation are those associated to the nominal, reference trajectories of the CubeSat and of the asteroid, and could be calculated and stored on the CubeSat's on-board computer prior to the mission. In such a way, propagation of the estimated trajectories can be performed simply by multiplying prestored state-transition matrices and the estimated deviations from the nominal trajectories (Eq. (5)).

$$\boldsymbol{x}_{est}(t_2) = \boldsymbol{x}_{nom}(t_2) + \underline{\boldsymbol{\phi}}_{nom}(t_2, t_1) \cdot \left(\boldsymbol{x}_{est}(t_1) - \boldsymbol{x}_{nom}(t_1)\right) \quad (5)$$

where the subscripts est and nom stand for variables evaluated along the estimated and nominal trajectories, respectively. While the process described in Eq. (5) provides less accurate results than numerical propagation of the equations of motion, it also reduces the on-board computational demand.

Analysis in [1] identified 41 asteroids that are reachable from L1/L2 within 150 days with 80 m/s of ΔV. A total ΔV budget of 80 m/s is also considered in this study, but shall also include trajectory correction maneuvers in addition to the nominal maneuvers to reach the asteroids. In order for at least 10 m/s of ΔV to be available for the TCMs, this study only analyzes asteroids that are reachable with less than 70 m/s of ΔV. Additionally, only asteroids that can be detected by the on-board star tracker more than 12 hours before the flyby are considered, since observing the asteroid for long enough is essential to achieve reasonable estimation accuracies. As a consequence of imposing these two additional constraints, only 18 out of the 41 asteroids identified in [1] are considered in this analysis.

4.1. Navigation strategy

The on-board navigation strategy consists of two phases: initially, (1) collecting observations of the Sun and visible planets after departure from L1/L2 until the asteroid becomes visible, and then, (2) collecting observations of the Sun and of the asteroid until the last trajectory correction maneuver is performed. Both navigation phases process observations through a least squares estimator [18], and the timeline of observations is summarized in Table 2.

During the first navigation phase, observations are used to estimate only the trajectory of the CubeSat. During the second navigation phase, the trajectories of the CubeSat and of the asteroid are simultaneously estimated instead.

The *a priori* estimation for the first navigation phase is the CubeSat's position and velocity along its nominal trajectory at the time of departure from L1/L2, and the *a priori* covariance matrix is that described in Section 3.1. During the second navigation phase, simultaneous estimation of the trajectories is performed by extending the estimated state vector through concatenation of the CubeSat's and asteroid's state vectors: $\boldsymbol{x}_{ext}$, and by building a 12x12 covariance matrix, $\underline{\boldsymbol{Q}}_{ext}$, such as that described in Eq. (6).

$$\boldsymbol{x}_{ext} = \begin{bmatrix} \boldsymbol{x}_{CubeSat} \\ \boldsymbol{x}_{asteroid} \end{bmatrix}$$
$$\underline{\boldsymbol{Q}}_{ext} = \begin{bmatrix} \underline{\boldsymbol{Q}}_{CubeSat} & \underline{\boldsymbol{0}}_{6x6} \\ \underline{\boldsymbol{0}}_{6x6} & \underline{\boldsymbol{Q}}_{asteroid} \end{bmatrix} \quad (6)$$

The resulting estimation from the first navigation phase is used as *a priori* estimation of the CubeSat's trajectory in the second navigation phase, and the nominal, reference trajectory of the asteroid is used as its *a priori* estimation. Lastly, the *a priori* covariance matrix associated to the asteroid is obtained as described in Section 3.4.

Corresponding propagations of the covariance matrices along time are performed employing Eq. (4) unless propulsive maneuvers are executed. In the presence of propulsive maneuvers, the CubeSat's covariance matrix is updated through Eq. (7) to account for maneuver execution errors [19,20]. Maneuver execution errors are introduced as process noise, $\underline{\boldsymbol{Q}}_{man}$, which is calculated as described in Section 3.2.

$$\underline{\boldsymbol{P}}(t_{man}^{+}) = \underline{\boldsymbol{P}}(t_{man}^{-}) + \underline{\boldsymbol{Q}}_{man} \quad (7)$$

where $\underline{\boldsymbol{P}}(t_{man}^{-})$ and $\underline{\boldsymbol{P}}(t_{man}^{+})$ are the covariance matrices before and after a maneuver executed at time t_{man}.

Another relevant aspect to the first navigation phase is deciding what planets should be observed and in which order. This decision is based upon the analysis in [21] that showed that best navigation accuracies are obtained by observing pairs of planets that are as close as possible to the observer and whose lines of sight are closest to 90 degrees.

A selection factor is introduced in [21] to determine which planets should be observed (see Eq. (8)), in terms of the sum of distances from the observer to the pair of planets (r_s), and the angle between the lines of sight, θ_s.

$$\text{Selection Factor} = \sin(\theta_s)/r_s \quad (8)$$

All combinations of two visible planets are considered, and their respective selection factors are computed at each of the observation times along the first navigation phase (Table 2). Pairs of planets with the highest selection factor are identified and selected for observation with the star tracker at two consecutive observation times. Visibility of planets is determined by their visual magnitude (V≤11) and shall avoid the solar exclusion area (40 degrees). If only one planet is visible, then that planet is observed, and if no planet is visible, then only sun sensor observations are collected. The sequence of planets to be observed is determined using the nominal trajectory of the CubeSat as reference, and could therefore be decided and stored in the on-board computer prior to the mission.

4.2. Guidance strategy

In contrast to the preliminary analysis in [2], where only one trajectory correction maneuver was performed at the end of the on-board navigation phase, two TCMs are considered in this study.

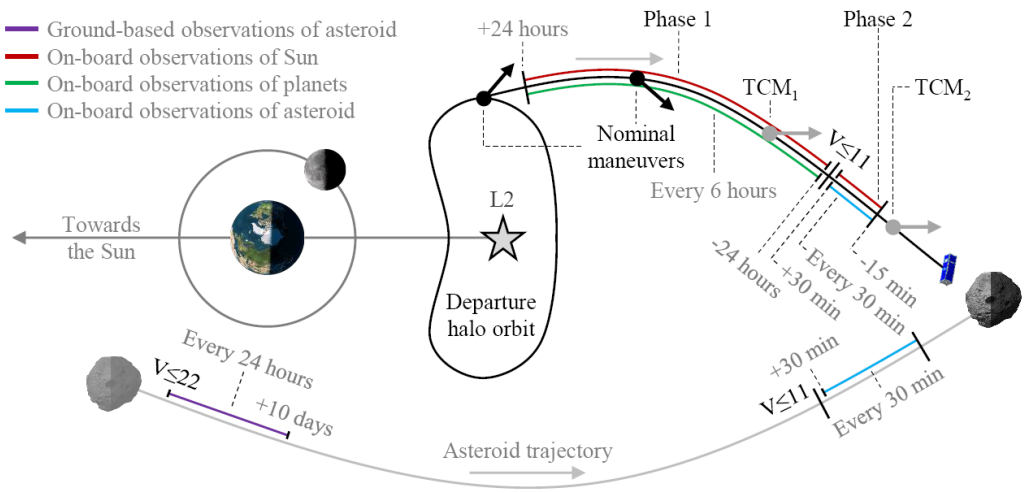

Fig. 4. Diagram of mission profile, including on-board navigation and guidance strategies

Analysis in [2] showed that final flyby accuracies are highly dependent on how long the asteroid can be observed by the CubeSat, since this will drive estimation accuracies. Given the low limiting magnitude of the star tracker, asteroids become visible only a few days prior to the flyby, and as a consequence, a large ΔV is required to correct the trajectory of the CubeSat.

The one-TCM guidance strategy analyzed in [2] showed stringent limitations in terms of (1) large ΔV requirements to correct the trajectory, and (2) high dependency on long asteroid observation times. In order to achieve flyby accuracies of the order of 100 km, the analysis in [2] imposed a requirement on the star tracker's limiting magnitude of V=15. Accomplishing this requirement, however, would involve long exposure times, high levels of noise, and a large number of visible stars. This would ultimately difficult the identification of star centroids and star patterns, and result in larger observation errors.

If a lower limiting magnitude of V=11 is assumed instead, asteroid observation times are reduced, hence decreasing estimation accuracies and increasing ΔV requirements. As a solution, a two-TCM guidance strategy is proposed in this study that enables the same flyby accuracies despite the shorter asteroid observation times, while maintaining ΔV requirements within the mission budget.

The guidance strategy here proposed employs two trajectory correction maneuvers: TCM_1 and TCM_2, one performed before the star tracker is able to detect the asteroid, and another one performed after collecting observations of the asteroid. TCM_1 is thus performed during the first on-board navigation phase (observations of Sun and planets), and TCM_2 is performed at the end of the second navigation phase (observations of Sun and asteroid). Illustrated in Fig. 4 is the whole mission profile, including the on-board navigation phases and the trajectory correction maneuvers.

The challenge that arises from this two-TCM strategy is deciding when these TCMs should be executed, and how much ΔV should be allocated to each of them. With the goal of achieving the same relative encounter point and time as in the nominal trajectories, a few factors should be considered to make this decision: (1) the later TCMs are executed, the better the estimation accuracy, (2) the sooner TCMs are executed, the lower the ΔV required to correct the trajectory, however, also (3) the sooner TCMs are executed, the larger the inaccuracies at the time of the flyby due to propagation of maneuver execution errors.

Taking these factors into consideration, a heuristic to decide the TCMs' execution time is developed based on the available ΔV, and on the information that can be provided by the dynamics' state-transition matrices and the estimation's covariance matrices. This decision is, furthermore, performed considering that both maneuvers are allocated as much ΔV as they require to correct the final position of the CubeSat, and in search of the latest TCM execution times that still fulfill the ΔV budget (for better estimation accuracies).

As a note, it is also worth clarifying that both maneuvers along the nominal trajectory (those computed in [1] and illustrated in Fig. 4) are executed as per design, and they are not recomputed by the on-board algorithms. The justification for this is twofold: (1) the quality of the estimation at the time of second nominal maneuver is generally not good enough to improve the final flyby accuracy, and (2) propagation of maneuver execution errors from the time of the second maneuver until the time of encounter also induce large inaccuracies.

The heuristic method considers only discrete possibilities for the times of execution of TCM_1 and TCM_2. On the one hand, possible execution times for TCM_1 are considered every 5 days before the asteroid is detected. Whereas possible execution times for TCM_2 are considered every 12 hours after asteroid detection. The

time of first asteroid detection ($V \leq 11$) is determined using the nominal CubeSat and asteroid trajectories.

At each of the possible TCM_1 execution times, the following steps are performed to select the fittest TCM_1 execution time:

(1) based on its current state estimate, the ΔV required to correct the final position of the CubeSat is computed (inverting Eq. (5)),
(2) based on its current estimation covariance matrix, which determines the accuracy of the ΔV computed in step (1), the covariance matrix at the time of the flyby is predicted, resulting from the hypothetical execution of TCM_1 and including asteroid ephemeris uncertainties at the time of the flyby and maneuver execution errors (Eq. (7) in combination with Eq. (4)),
(3) for each of the possible TCM_2 execution times, and assuming TCM_1 was already executed, the ΔV required to correct the largest semi-axis in position of the 3-σ covariance matrix predicted in step (2) is calculated (inverting Eq. (5)), and
(4) the ΔV requirements computed in steps (1) and (3) are added together and compared to the remaining ΔV after the nominal maneuvers.

In this way, at each of the possible TCM_1 execution times, and assuming TCM_1 is executed then, it is possible to estimate the total ΔV required to correct the trajectory depending on when TCM_2 is executed. The latest TCM_2 execution time fulfilling the mission's ΔV budget can be identified, and is stored for decision-making.

If this procedure is performed for all possible TCM_1 execution times, it will be observed that, initially, delaying TCM_1 also allows to delay TCM_2 as a result of improving the estimation accuracy along the first on-board navigation phase, and, eventually, delaying TCM_1 requires TCM_2 to be executed earlier in order to remain within the ΔV budget. The fittest solution is thus identified as the TCM_1 that allows for the latest TCM_2.

In order for this heuristic to be suitable for an autonomous CubeSat, however, at each possible TCM_1 execution time, it would be necessary to predict what the latest possible TCM_2 will be at the next TCM_1 execution time. And, eventually, TCM_1 will be performed when TCM_2 needs to be performed earlier at the next TCM_1 execution time than at the current time. Prediction of the latest possible TCM_2 at the next TCM_1 time involves completing steps (1–4) based only on the information available until the current TCM_1 time. This prediction thus requires an estimation of the state and of the estimation's covariance matrix at the next TCM_1 time.

A prediction of the state is obtained simply forward-propagating the estimated state at the current time (Eq. (5)). In order to predict the covariance matrix, it can be noticed that the size of the estimation's covariance matrix (eigenvalues) describes a decreasing "S"-shaped or sigmoid curve along the first on-board navigation phase, whereas the orientation (eigenvectors) is constant. Therefore, previous sizes of the covariance matrix can be used to approximate the eigenvalues of the following covariance matrix. For simplicity, in this study, the covariance matrix at the following TCM_1 time is linearly approximated employing only the eigenvalues of the current and of the immediately previous covariance matrices.

Selection of TCM_2's execution time is performed during the second on-board navigation phase, employing the information available from the relative optical navigation. At each of the possible TCM_2 execution times, the state at the next possible TCM_2 time is predicted, based on the current state estimate (applying Eq. (5)), and, assuming TCM_2 is executed then, the ΔV required to achieve the same relative flyby position as in the nominal trajectories is computed (inverting Eq. (5)). If the ΔV requirement at the next possible TCM_2 execution time is larger than the remaining ΔV, then TCM_2 is executed at the current execution time.

5. Analysis and discussion

Analysis shows that small uncertainties in asteroid ephemeris are essential for the success of the mission. Although asteroid ephemeris uncertainties are reduced through relative optical navigation in the second on-board navigation phase, only certain levels of ephemeris uncertainties can be mitigated. A first step in the mission analysis is, therefore, modeling the accuracy in asteroid ephemeris that will be available prior to the mission.

5.1. Ground-based observation campaign

As described in Section 3.4, asteroid ephemerides are improved prior to the mission through a ground-based observation campaign if the asteroids are visible from Earth ($V \leq 22$). Adding more recent observations to the estimation process increases the observed arc length of the asteroid's orbit (time between first and last observations), and as a result, the uncertainty in asteroid ephemeris tends to decrease. This decreasing tendency in ephemeris uncertainty with arc length was analyzed in [17] and described by a piecewise linear function in a logarithmic scale. Four different sections are identified in this tendency depending on the asteroids' observed arc length [17]: below 10 days, between 10 and 250 days, between 250 and 8000 days, and above 8000 days.

New ground-based observations are modeled and processed as described in Section 3.4, and comparison to the expected piecewise linear behavior is used a means of verification that realistic levels of uncertainty are obtained after the ground-based observation campaign. Analysis shows that a decrease in ephemeris uncertainty consistent with the analysis in [17] is in fact obtained when simulating ground-based observations (see Fig. 5).

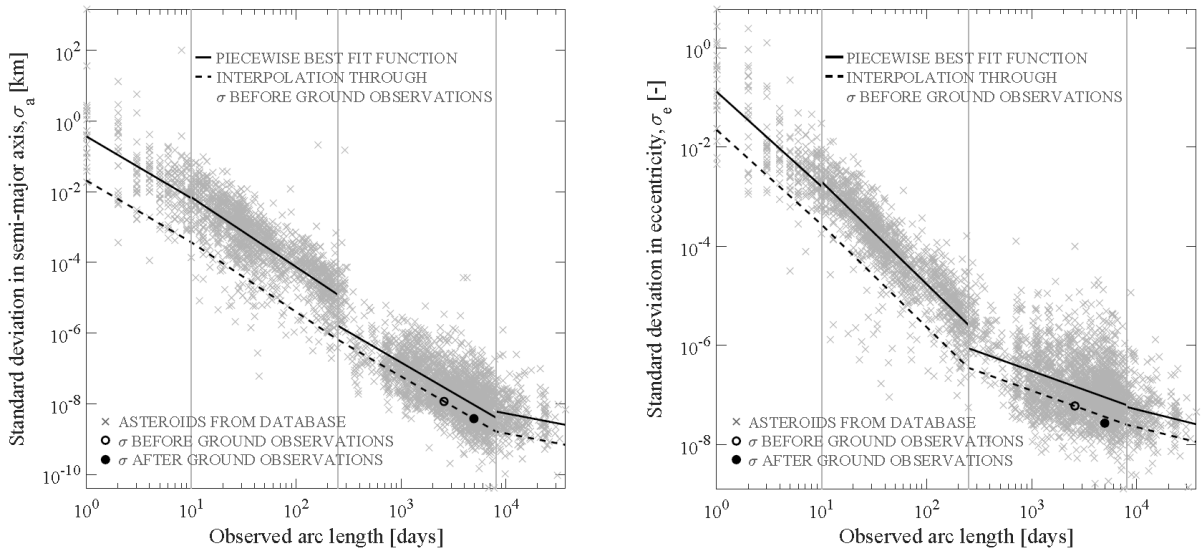

Fig. 5. Keplerian element uncertainty for asteroid 2005 WD before and after collecting ground-based observations

Table 3. Asteroid flyby trajectory characteristics and results from ground-based observations

		Nominal trajectory characteristics		**Improvement through ground observations**	
Asteroid	**From**	**Visible days from CubeSat**	**ΔV range from L1/L2 (m/s)** [1]	**Observed arc length (days)**	**3σ uncertainty at time of flyby (km)**
2005 WD		0.8	59.1↔69.2	2565→4956	96.9→82.6
2015 BK509[a,b]		0.8	47.2	27	3442334.0
2008 TZ3		7.1	42.5↔56.9	3632→4068	37.5→37.3
2017 XC62		2.4	26.0↔60.5	176→1348	120860.8→499.6
2008 DG5[b]		2.6	32.8	6494→7945	178.2→173.0
1997 NC1	L2	0.6	15.6↔68.2	7681→10234	248.8→223.6
2012 EY11[b]		12.4	68.2	5902→9513	363.1→279.4
2001 SQ3		0.6	38.4↔68.3	4518→7730	282.3→277.0
2001 WN5[c]		3.8	44.1↔65.0	8463→11325	231.8→221.9
2004 OB[b]		1.5	36.4	5447→8745	239.7→222.0
2004 MN4[c]		2.6	5.7↔57.6	3946→9009	14.7→14.6
2001 FO32		2.2	30.5↔62.8	5009→7216	849.9→598.9
2014 HK129[b]		18.4	47.3	528→3004	35084.4→791.2
2010 XC15[a,b]		0.6	26.7	2549	484.9
2018 CC14[b]	L1	0.6	68.5	101→2094	3018731.6→313.8
2001 WN5[c]		1.0	4.4↔40.3	8463→8700	233.6→170.0
2009 BL71		0.9	20.3↔50.3	3716→6961	174.7→142.4
2004 MN4[c]		7.3	20.9↔50.7	3946→9121	241.6→220.3

[a] Asteroid ephemerides cannot be improved since they are not observable from Earth prior to the mission.
[b] Reachable with <70 m/s from only one of the nine departure points along the halo orbit considered in [1].
[c] Asteroid 2001 WN5 can be reached from L1 and L2. Ephemeris uncertainties are larger for a flyby from L2 as a consequence of the asteroid's close encounter with Earth. Same applies to asteroid 2004 MN4 (Apophis) from L1.

As an example, illustrated in Fig. 5 are the resulting uncertainties at the time of the flyby in the Keplerian semi-major axis and eccentricity elements before and after collecting ground-based observations of asteroid 2005 WD. It is observed that the decrease in these uncertainties is comparable to the general tendency of the best-fit piecewise function relating ephemeris uncertainty and arc length. This analysis, and the calculation of the best-fit piecewise function, considers only asteroids with similar characteristics to the target asteroids described in Section 2 and in [1]: asteroids larger than 100 meters in diameter that fly close to the Earth (within 0.1 au) between years 2019 and 2030.

Table 3 summarizes the results of collecting ground-based observations of the asteroids considered in this analysis. Only asteroids listed in [1] that are reachable

with less than 70 m/s and that are visible by the CubeSat for more than 12 hours are considered, as mentioned in Section 4. Observed arc lengths before and after collecting ground-based observations are summarized in Table 3, as well as the corresponding ephemeris uncertainties at the time of the flyby (represented by the largest semi-axis of the 3σ covariance matrix). It is observed that significant improvements in uncertainty are obtained for asteroids with low arc lengths prior to new ground observations, for which uncertainties above 10,000 km are reduced below 1000 km. This improvement is less prominent, however, if <1000-km uncertainties were already available.

It can thus be concluded that a ground-based observation campaign is essential for asteroids with large ephemeris uncertainties, since the observation campaign can significantly decrease this uncertainty. Otherwise, uncertainty improvements may not be substantial and an observation campaign before the mission may not be strictly necessary.

5.2. Monte Carlo analysis

Monte Carlo simulations (10,000 runs) are carried out to understand the flyby accuracies that can be achieved through the autonomous navigation and guidance strategy described in Section 4. Simulations are performed for two cases per asteroid: (1) departure point from L1/L2 with smallest ΔV requirement, and (2) departure point from L1/L2 with largest ΔV requirement below 70 m/s (listed in Table 3).

Results of the two-TCM guidance strategy described in Section 4.2 are compared to the results of two more guidance scenarios: (1) guidance strategy with only one TCM (such as that employed in [2]), and (2) scenario where no TCMs are performed, which illustrates the deviations produced by execution errors in the nominal propulsive maneuvers. In the one-TCM strategy, selection of the TCM execution time is performed following the same procedure as for TCM_2 in the two-TCM guidance strategy (Section 4.2): predicting the ΔV cost at the next possible TCM execution time until that cost exceeds the available ΔV budget.

As an example of the results obtained through these three guidance strategies, Fig. 6 illustrates the B-plane error ellipses for asteroid 2017 XC62, along with the error ellipse that would be obtained if only one TCM was performed at the end of the first on-board navigation phase. This last guidance scenario exemplifies the flyby accuracies that would be obtained if no on-board observations of the asteroid were collected.

It is observed in Fig. 6 that flyby errors of the order of tens of thousands kilometers would be obtained if no TCMs were performed. Slightly smaller but still unreasonably large errors would be obtained if no relative optical navigation was performed. Lastly, it is also observed how the two-TCM guidance strategy introduced in this study delivers flyby accuracies approximately one order of magnitude better than those obtained with only one TCM.

As another example of the importance of the relative navigation phase, Fig. 7 illustrates the evolution along time of the estimation error of the relative CubeSat-asteroid position vector at the time of the flyby, for asteroid 2017 XC62. It is clearly observed in Fig. 7 how the estimation error is reduced by approximately one order of magnitude as the first observations of the asteroid are collected.

Similar tendencies to those illustrated in Fig. 6 and Fig. 7 are obtained for asteroids listed in Table 3. Table 4 is provided to summarize the flyby accuracies that can be achieved through the guidance strategies considered here, along with the relative estimation error at the time of the flyby. All uncertainties in Table 4 are represented by the largest semi-axis in position of the corresponding 3σ covariance matrices.

Several observations can be made from the results in Table 4, together with the ΔV and visibility information in Table 3, namely:

- the two-TCM guidance strategy introduced here provides results approximately one order of magnitude better than a one-TCM strategy: e.g., for asteroid 2008 TZ3, flyby accuracies below 100 km can be obtained through the two-TCM strategy, whereas accuracies above 1000 km are obtained through the one-TCM strategy.
- missions of shorter duration result in better flyby accuracies since time for error propagation is reduced: e.g., better flyby accuracies are obtained for asteroid 2001 FO32 along the 78.1-day flyby trajectory despite having a larger nominal ΔV requirement (62.8 m/s) than the 150-day trajectory (30.5 m/s). This is also observed in the no-TCM results, which are significantly better for the 78.1-day trajectory.
- uncertainty in asteroid ephemeris prior to the mission largely drives the resulting flyby accuracies: e.g., worst flyby accuracies are obtained for asteroid 2015 BK509 whose ephemeris uncertainty is the largest, and best flyby accuracies are obtained for asteroid 2004 MN4 whose ephemeris uncertainty is the smallest.
- early detection of the asteroid is essential to reduce estimation errors and, effectively, resulting flyby accuracies: e.g., asteroid 2001 SQ3 is observed only 0.6 days before the flyby and results in estimation and flyby accuracies are one order of magnitude larger than those of asteroid 2012 EY11, which is observed for 12.4 days and has a large nominal ΔV requirement (68.2 m/s).

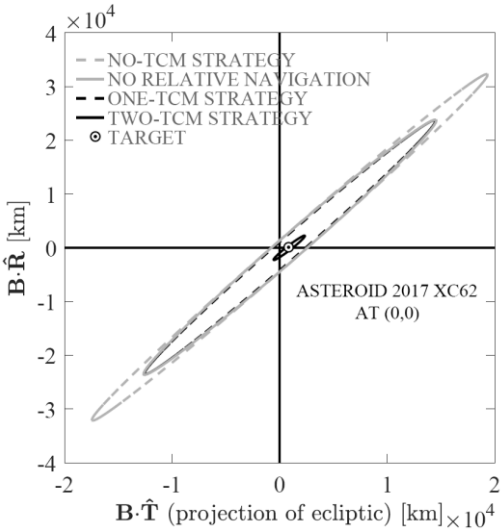

Fig. 6. B-plane 3σ error ellipses for asteroid 2017 XC62 depending on guidance strategy

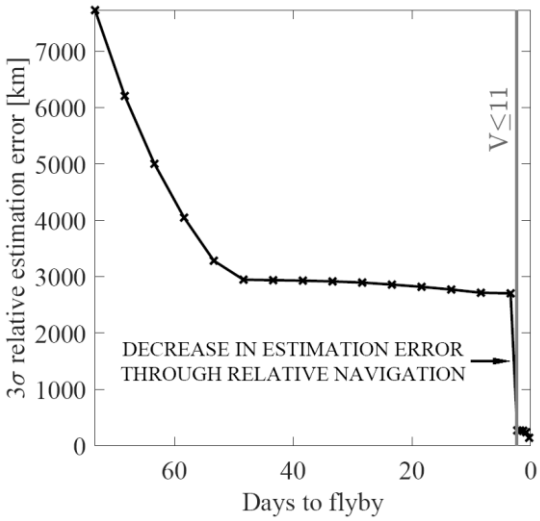

Fig. 7. Evolution of relative estimation error for asteroid 2017 XC62 as a function of time

Table 4. Flyby trajectory characteristics and results from ground-based observations

Asteroid	Mission duration (days)	Range in 3σ flyby accuracies (km)			Range in 3σ relative estimation error at time of flyby (km)
		Two-TCM strategy	One-TCM strategy	No-TCM strategy	
2005 WD	141.7↔150.0	32958.3↔37021.3	43751.9↔41942.5	51139.4↔45847.1	1051.3↔266.6
2015 BK509	150.0	3217339.1	3218001.3	3218169	35405109.1
2008 TZ3	129.7↔149.9	25.8↔38.0	1864.3↔9135.8	20383.8↔29284.7	8.5↔9.7
2017 XC62	150.0↔141.8	71.9↔2664.2	17659.0↔27199.0	40715.1↔37112.3	4.3↔17.9
2008 DG5	138.0	264.2	7561	27276.1	8.6
1997 NC1	140.4↔81.0	4751.9↔7349.9	19275.6↔10581.6	32335.8↔12929.6	4.5↔1068.8
2012 EY11	150.0	356.6	16748.7	40867.4	46.4
2001 SQ3	140.7↔124.5	3100.2↔22811.4	21899.6↔32037.3	33513.7↔35549.3	687.0↔935.6
2001 WN5	150.0↔115.5	1261.8↔906.1	7683.8↔1958.7	11641.9↔3112.3	111.0↔55.0
2004 OB	149.6	1911.6	11745.7	20364.9	124.6
2004 MN4	140.2↔55.9	9.6↔15.7	22998.6↔22.5	40765.8↔2694.2	2.9↔4.7
2001 FO32	150.0↔78.1	1381.2↔57.4	50905.1↔1934.7	71579.3↔8237.7	40.6↔18.9
2014 HK129	150	14	286.7	21857.4	4.5
2010 XC15	141.2	188.9	54735.5	69068.1	45.4
2018 CC14	141.6	1008.6	30571.6	33835.5	64.8
2001 WN5	33.3↔149.9	13.5↔12.1	13.7↔9385.9	442.8↔12300.5	4.5↔4.0
2009 BL71	150.0↔110.8	20.8↔12.7	41952.9↔11988.6	57148.0↔20217.8	5.1↔4.1
2004 MN4	125.8↔33.3	7.9↔9.5	340.2↔15.5	8780.4↔1314.2	2.6↔3.1

- lower nominal ΔV requirements from L1/L2 result in better flyby accuracies since a larger ΔV is available for TCMs, and, as a consequence, TCMs can be executed at a later time thus reducing relative estimation errors: e.g., better estimation errors and flyby accuracies are obtained for asteroid 2017 XC62 along the 26.0-m/s flyby trajectory than along the 60.5-m/s trajectory, despite having a longer duration (150 days) and larger no-TCM flyby error.

Through this Monte Carlo analysis, it is thus seen that flyby accuracies well below 100 km can be achieved through autonomous navigation if the two-TCM strategy introduced here is employed.

The main advantage of this two-TCM guidance strategy is that deviations from the designed, nominal trajectory are initially reduced along the first on-board navigation phase (through TCM_1, which has a low ΔV cost). As a consequence of TCM_1, a smaller ΔV is then required to correct the trajectory during the second on-board navigation phase. Reducing the ΔV demand on TCM_2 allows for a later execution of TCM_2 which increases asteroid observation times. Observing the

asteroid for a longer time reduces estimation errors and, ultimately, this results in better flyby accuracies.

In terms of the systems requirements, the two-TCM guidance strategy allows for better flyby accuracies for a given ΔV budget, and it also allows for a smaller limiting magnitude of the star tracker. Additionally, as mentioned in Section 4, the navigation and guidance algorithms propagate trajectories and compute velocity corrections employing only prestored state-transition matrices in the interest of the limited computational power on board the CubeSat.

Even though the two-TCM strategy presents significant advantages over the one-TCM strategy employed in [2], proper flyby accuracies can only be achieved if a suitable combination of (a) asteroid visibility time, (b) remaining ΔV for TCMs, (c) *a priori* asteroid ephemeris uncertainty, and (d) mission duration is available. For reference, flyby accuracies below 100 km can only be achieved for 8 out of the 41 asteroids that were identified as reachable in [1]. In order to increase the number of asteroids with acceptable flyby accuracies, some of the mission requirements would have to be relaxed either increasing the size and capability of the spacecraft, or including radiometric observations for navigation (thus reducing the autonomy of the mission).

Conclusions

This study presents a feasibility analysis of an autonomous 3U CubeSat mission to an asteroid. The mission concept considers a CubeSat departs from a halo orbit around the Sun-Earth barycentric Lagrange points and performs autonomous navigation and guidance to flyby an asteroid.

The autonomous navigation strategy considered here consists of two phases: (1) observations of visible planets and of the Sun until the target asteroid becomes visible, and (2) observations of the Sun and of the asteroid for relative optical navigation. The guidance strategy employs two trajectory correction maneuvers to improve the flyby accuracies: one during the first navigation phase, and another one during the second on-board navigation phase.

A heuristic to compute the time of execution of each correction maneuver that is suitable for an autonomous CubeSat is introduced, and Monte Carlo simulations are performed to understand the flyby accuracies that can be achieved. Realistic system specifications are modeled as well as uncertainties in asteroid ephemeris.

Flyby accuracies well below 100 km are found possible if the mission characteristics are suitable in terms of: (a) asteroid visibility time, (b) available ΔV for trajectory correction maneuvers, (c) uncertainty in asteroid ephemeris prior to the mission, and (d) mission duration. Results of the two-TCM guidance strategy introduced here show significant advantages over a one-TCM strategy, both in terms of flyby accuracies for a given ΔV budget and in terms of limiting magnitude for the on-board navigation camera.

However, the number of reachable asteroids for which <100-km flyby accuracies are possible is limited, and improving these results would require a larger CubeSat or SmallSat platform or partial navigation support from ground stations.

Ultimately, this study provides a high-fidelity feasibility analysis of asteroid flyby missions using autonomous CubeSats. An autonomous navigation and guidance strategy is proposed and proven effective despite the demanding mission characteristics, and its limitations are identified.

References

[1] P. Machuca, J.P. Sánchez, High-fidelity trajectory design to flyby near-Earth asteroids using CubeSats, Acta Astronaut. (2019).

[2] P. Machuca, J.P. Sánchez, S. Greenland, Asteroid flyby opportunities using semi-autonomous CubeSats: Mission design and science opportunities, Planet. Space Sci. 165 (2019) 179–193. doi:10.1016/j.pss.2018.11.002.

[3] K. Lemmer, Propulsion for CubeSats, Acta Astronaut. 134 (2017) 231–243. doi:10.1016/j.actaastro.2017.01.048.

[4] S. Campagnola, N. Ozaki, Y. Sugimoto, C.H. Tam, H. Chen, Y. Kawabata, S. Ogura, B. Sarli, Y. Kawakatsu, R. Funase, S. Nakasuka, Low-thrust Trajectory Design and Operations of PROCYON, the First Deep-Space Micro-Spacecraft, in: Int. Astronaut. Congr., Jerusalem, Israel, 2015.

[5] L. Mcnutt, L. Johnson, D. Clardy, Near-Earth Asteroid Scout, in: AIAA Sp. 2014 Conf. Expo., 2014: pp. 1–9. doi:10.2514/6.2014-4435.

[6] CU Aerospace, Propulsion Unit for CubeSats, Champaign, IL, USA, 2017.

[7] M. Armanoa, H. Audleyb, G. Augerc, J. Bairdn, P. Binetruyc, M. Bornb, D. Bortoluzzid, A Strategy to Characterize the LISA-Pathfinder Cold Gas Thruster System, J. Phys. Conference (2015). doi:10.1088/1742-6596/610/1/012026.

[8] G. Anderson, J. Anderson, M. Anderson, G. Aveni, D. Bame, P. Barela, K. Blackman, A. Carmain, L. Chen, M. Cherng, S. Clark, M. Connally, W. Connolly, D. Conroy, M. Cooper, C. Cutler, J.D. Agostino, N. Demmons, E. Dorantes, C. Dunn, M. Duran, E. Ehrbar, J. Evans, J. Fernandez, G. Franklin, M. Girard, J. Gorelik, V. Hruby, O. Hsu, D. Jackson, S. Javidnia, D. Kern, M. Knopp, R. Kolasinski, C. Kuo, T. Le, I. Li, O. Liepack, A. Littlefield, P. Maghami, S. Malik, L. Markley, R. Martin, J. Mehta, J. Mennela, D. Miller, D. Nguyen, J.O. Donnell, R. Parikh, G. Plett, T. Ramsey, T.

Randolph, S. Rhodes, T. Roy, A. Ruiz, H. Shaw, J. Slutsky, D. Spence, J. Stocky, J. Tallon, I. Thorpe, W. Tolman, H. Umfress, R. Valencia, C. Valerio, W. Warner, J. Wellman, P. Willis, J. Ziemer, J. Zwahlen, S.T. Team, Experimental results from the ST7 mission on LISA Pathfinder, Phys. Rev. 98 (2018). doi:10.1103/PhysRevD.98.102005.

[9] J.E. Pollard, Beam-Centroid Tracking Instrument for Ion Thrusters, El Segundo, CA, USA, 1995.

[10] S. Palo, G. Stafford, A. Hoskins, An Agile Multi-use Nano Star Camera for Constellation Applications, in: Small Satell. Conf., 2013.

[11] J.P. Mason, M. Baumgart, B. Rogler, C. Downs, M. Williams, T.N. Woods, S. Palo, P.C. Chamberlin, S. Solomon, A. Jones, X. Li, R. Kohnert, A. Caspi, MinXSS-1 CubeSat On-Orbit Pointing and Power Performance: The First Flight of the Blue Canyon Technologies XACT 3-axis Attitude Determination and Control System, J. Small Satell. (2017). http://arxiv.org/abs/1706.06967.

[12] Hyperion Technologies B.V., Hyperion Technologies SS200 Sun Sensor, Delft, Netherlands, 2017.

[13] V. Franzese, P. Di Lizia, F. Topputo, Autonomous Optical Navigation for LUMIO Mission, 2018 Sp. Flight Mech. Meet. (2018). doi:10.2514/6.2018-1977.

[14] H.H. Ku, Notes on the Use of Propagation of Error Formulas, J. Res. Natl. Bur. Stand. (1934). 70C (1966) 263–273.

[15] NASA, JPL HORIZONS, (2013). http://ssd.jpl.nasa.gov/?horizons (accessed January 1, 2018).

[16] European Space Agency, NEODyS-2, (2011).

[17] J. Desmars, D. Bancelin, D. Hestroffer, W. Thuillot, J. Desmars, D. Bancelin, D. Hestroffer, W.T. Statistical, J. Desmars, D. Bancelin, D. Hestro, W. Thuillot, Statistical and Numerical Study of Asteroid Orbital Uncertainty, Astron. Astrophys. A32 (2013).

[18] W.E. Wiesel, Modern Orbit Determination, 2nd ed., Aphelion Press, Beavercreek, OH, USA, 2003.

[19] A. Gelb, J.F. Kasper, R.A. Nash, C.F. Price, A.A. Sutherland, Applied Optimal Estimation, The M.I.T. Press, 1974.

[20] C. Schiff, Adapting Covariance Propagation to Account for the Presence of Modeled and Unmodeled Maneuvers, in: AIAA/AAS Astrodyn. Spec. Conf. Exhib., American Institute of Aeronautics and Astronautics, 2006. doi:doi:10.2514/6.2006-6294.

[21] B.Y. Kawabata, Y. Kawakatsu, On-board Orbit Determination using Sun Sensor and Optical Navigation Camera for Deep-Space Missions, 15 (2017) 13–19.